J. Fluid Mech. (2015), *vol.* 767, *pp.* 85–94.
doi:10.1017/jfm.2014.742

Inertial effects on the generation of co-laminar flows

William A. Braff[1,2], **Martin Z. Bazant**[3] **and Cullen R. Buie**[2,†]

[1]Giner Inc., Newton, MA 02466, USA

[2]Department of Mechanical Engineering, Massachusetts Institute of Technology, Cambridge, MA 02139, USA

[3]Departments of Chemical Engineering and Mathematics, Massachusetts Institute of Technology, Cambridge, MA 02139, USA

(Received 7 January 2014; revised 7 December 2014; accepted 21 December 2014)

The assumption of low Reynolds number flow, or Stokes flow, is often applied to the understanding of a broad range of microfluidic devices, including micro-reactors, biomedical devices, and membraneless electrochemical cells. However, recent studies have shown that various inertial effects can play a significant role, even in microfluidic systems. In this work, two- and three-dimensional secondary flows are identified in a generic rectangular flow channel design consisting of a secondary channel feeding fluid into a main channel. We identify a scaling argument which is able to predict the occurrence of these secondary flows as a function of system parameters. The impact of these behaviours on the assumption of fully developed colaminar flow is investigated. This work considers a representative geometry, and identifies a set of conditions where inertial effects can play a key role in a microfluidic device.

Key words: laminar reacting flows, microfluidics, micro-/nano-fluid dynamics

1. Introduction

Early applications of microfluidics often combined multiple fluid streams under conditions of laminar flow, with applications ranging from flow cytometry (Eyal & Quake 2002) to micro-reactors (Kenis, Ismagilov & Whitesides 1999). In these systems, moderate Reynolds numbers ($Re < 3000$) inhibit turbulent flow, ensuring that fluids mix only due to molecular diffusion. Further, Stokes flow is often assumed, allowing boundary layer analyses to describe some aspects of mixing (Ismagilov *et al.* 2000; Sprague & Dutta 2012; Thorson *et al.* 2012; Braff, Bazant & Buie 2013*a*; Braff, Buie & Bazant 2013*c*). In practice, the Reynolds number in many of these devices is of order unity or greater. As long as the flow is fully developed and unidirectional, this is irrelevant since the velocity and the velocity gradient are orthogonal, eliminating inertial effects. However, when the flow bends, or if two channels converge into one, these effects no longer disappear, and must be taken into account.

† Email address for correspondence: crb@mit.edu

The role of inertia in microfluidics has been previously examined in the context of flow in curved channels (Dean 1927; Berger, Talbot & Yao 1983; Di Carlo 2009; Mao *et al.* 2012; Norouzi & Biglari 2013). Asymptotic expansions have been calculated for very specific cases, including flow in a curved rectangular channel (Norouzi & Biglari 2013), but most efforts have been numerical (Guglielmini *et al.* 2010) or experimental (Van Hirtum, Grandchamp & Cisonni 2012). There has also been some investigation of geometrically induced inertial recirculation created by sharp corners that lead to flow separation (Chiu 2006; Sudarsan & Ugaz 2006). Inertia has also been identified as playing a role in common inlet geometries where multiple streams converge, but questions remain (Gambin *et al.* 2011; Nasir *et al.* 2011). In this work, we examine the role of inertia around the inlet of two channels coming together under a range of conditions, taking existing experimental inlet designs used in membraneless electrochemical cells as a template (Jayashree *et al.* 2005, 2010; Salloum & Posner 2010; Braff *et al.* 2013*a*; Braff, Buie & Bazant 2013*b*). These systems rely on reactant separation to successfully generate power. Fully developed unidirectional flow ensures reactant separation, but the extent to which this assumption breaks down near the inlet is not well understood, and has not been considered in past investigations of membraneless electrochemical systems (Braff *et al.* 2013*b*).

In this work, the Navier–Stokes equations are solved numerically for two- and three-dimensional geometries describing the flow of a fluid introduced into a main channel via an angled inlet. The geometry of this system mimics that of a membraneless laminar flow battery presented experimentally elsewhere (Braff *et al.* 2013*a*). Two major sources of mixing are identified: recirculation at the inlet junction due to flow separation, and fluid mixing perpendicular to the flow direction due to three-dimensional wall effects. We find that under certain conditions, these two effects drastically increase mixing beyond what would be predicted in a fully developed unidirectional system. A number of mitigation strategies are presented and discussed, and a scaling analysis is performed to better understand the underlying physics. To our knowledge, the scaling analysis herein is the first attempt to predict the onset of separation and secondary flows at the intersection of microchannels at moderate *Re*.

2. Numerical solution

Two- and three-dimensional domains were modelled, as shown in figure 1. The fluid flow was modelled using the Navier–Stokes equation, and mass transport was overlaid onto the results of that solution using dilute solution theory in a Newtonian fluid. The complete set of governing equations solve for the velocity field $\boldsymbol{v}$, pressure P, and concentration c in terms of fluid density ρ, viscosity μ, and diffusion coefficient D:

$$\rho\left(\frac{\partial \boldsymbol{v}}{\partial t}+\boldsymbol{v}\cdot\boldsymbol{\nabla}\boldsymbol{v}\right)=\mu\nabla^2\boldsymbol{v}-\boldsymbol{\nabla}P, \tag{2.1a}$$

$$\frac{\partial c}{\partial t}+\boldsymbol{v}\cdot\boldsymbol{\nabla}c=D\nabla^2 c. \tag{2.1b}$$

Steady state was assumed in all cases, so the time-dependent partial derivative drops out of the equations. No slip and no flux were assumed along the walls of the channel. In the three-dimensional model, only half the width of the channel was modelled, with a symmetry boundary condition imposed at the centreline.

The system was implemented in COMSOL Multiphysics (Burlington, MA). The flow remains laminar because the Reynolds numbers investigated were sufficiently low.

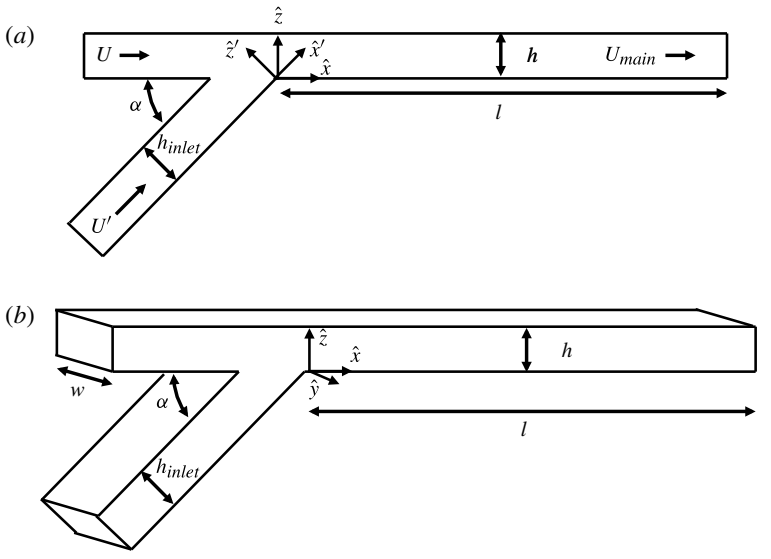

FIGURE 1. Flow cell geometry in the (*a*) two-dimensional and (*b*) three-dimensional domain.

Parameter (units)	Symbol	Value
Channel width (mm)	w	1.8
Channel length (cm)	l	1.3
Main channel height (μm)	h	100
Secondary channel height (μm)	h_{inlet}	300
Secondary channel angle (deg.)	α	45
Fluid density (kg m^{-3})	ρ	10^3
Fluid viscosity (Pa s)	μ	10^{-3}
Diffusion coefficient (cm^2 s^{-1})	D	10^{-5}
Volumetric flow ratio	n	10

TABLE 1. Parameters employed in the numerical calculation unless otherwise specified.

Numerical parameters were chosen to match previous experimental data, and unless otherwise specified are listed in table 1. To be consistent with past experimental work, the volumetric flow ratio n between the inlet to the main channel and the inlet to the secondary channel was maintained at 10:1, with a dimensionless concentration of one maintained at the beginning of the secondary channel. The flow rates were set to ensure that once the channels converged, the average flow velocity in the main channel, U_{main}, resulted in the specified Reynolds number, expressed in terms of the fluid density ρ, fluid viscosity μ, and channel height h:

$$Re = \frac{\rho U_{main} h}{\mu}. \tag{2.2}$$

3. Results and discussion

It is useful to compare the numerical results with those assuming fully developed unidirectional flow. In this case species transport is modelled by assuming unidirectional Poiseuille flow in a channel with perfectly divided reactant starting at

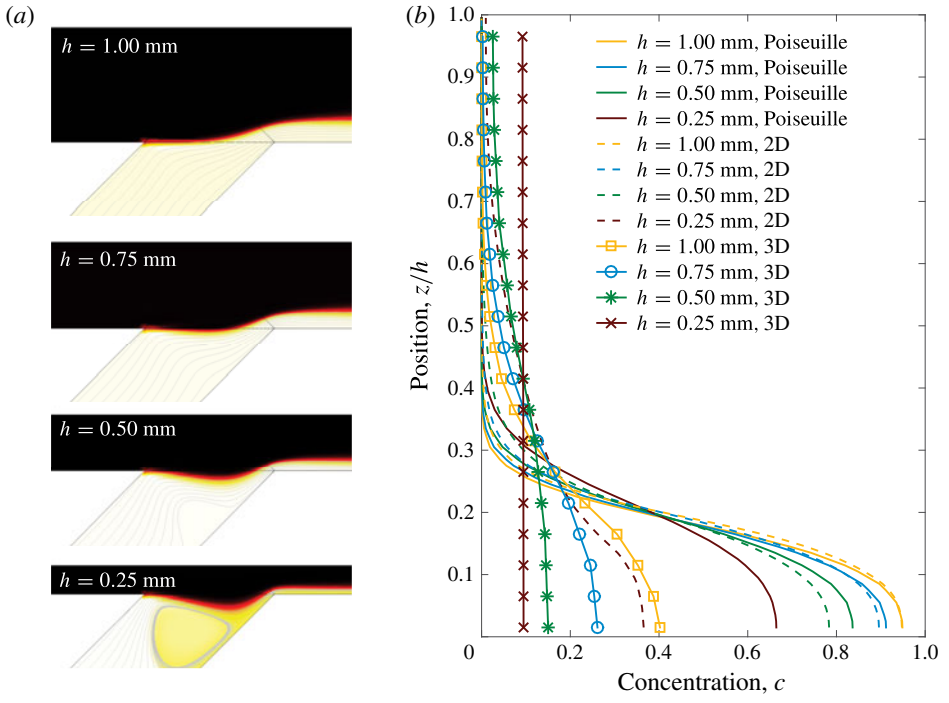

FIGURE 2. (Colour online) (*a*) Species concentration distribution and fluid stream lines for two-dimensional flow near the inlet as a function of channel height for a Reynolds number of 10. All other parameters are specified in table 1. For sufficiently thin channels, flow separation and recirculation can be observed. (*b*) Species concentration at the main channel outlet ($x/L = 1$) centreline as a function of channel height for fully developed Poiseuille flow, a two-dimensional inlet, and a three-dimensional inlet geometry with other parameters as specified in table 1. In the absence of flow recirculation, the two-dimensional model produces results similar to those predicted by ideal Poiseuille flow, but recirculation significantly enhances mixing. The three-dimensional channel produces significantly more mixing, with significant mass reaching the far wall for channels as tall as 500 μm.

$x = 0$ in the channel, as might be ideally assumed for the geometry shown in figure 1. In such a system, the reactant concentration profile at the inlet of the channel could be assumed to be an idealized step function, while the flow could be treated as perfectly unidirectional Poiseuille flow. Under these idealized conditions, there would be no advection of reactant across the channel, and reactant diffusion across the channel is sufficiently slow that almost none of it reaches the opposite side of the channel by the time it reaches the outlet, as shown in figure 2. This condition is necessary for a number of applications, and would indicate that if inertial effects can be neglected, channel heights as small as 250 μm are feasible.

Two-dimensional numerical calculations were performed for a range of channel heights, from 1 mm down to 250 μm, as shown in figure 2. For channel heights greater than 500 μm, the fluid from the secondary channel appears to flow smoothly into the main channel, with minimal disturbance in the flow near the inlet. This results in strong species separation at the outlet of the channel consistent with the fully developed case. As the channel height shrinks to 500 μm, however, significant

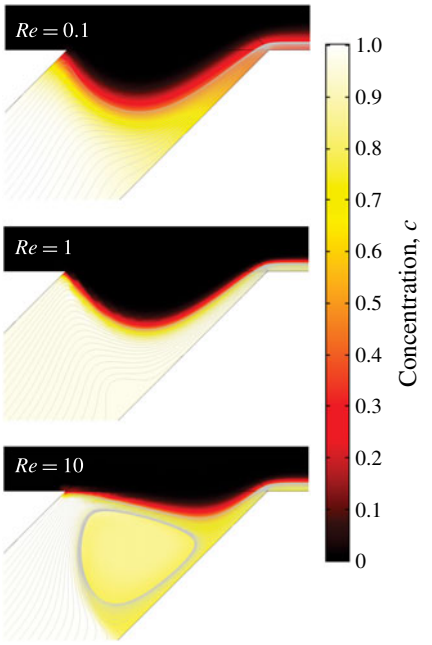

FIGURE 3. (Colour online) Species concentration near the inlet of the two-dimensional channel with a height of 250 μm as a function of Reynolds number. Under the conditions specified in table 1, Reynolds numbers of 0.1, 1, and 10 correspond to effective inlet Reynolds numbers of 0.3, 3, and 30, respectively. As the Reynolds number increases, the velocity gradient near where the secondary channel meets the main channel is enhanced, resulting in flow deformation and recirculation.

flow deformation is observed in the inlet. At 250 μm, flow recirculation is observed in the secondary channel, resulting in dramatically increased mixing, and diminished species separation at the outlet of the main channel. This recirculation behaviour is a function of the Reynolds number in the system, indicating that it is inertial in nature, as shown in figure 3. This type of steady recirculation behaviour is also commonly observed in flow along curved surfaces when the Reynolds number is between 4 and 40 (Kundu, Cohen & Dowling 2012).

Greater understanding of the physics leading to recirculation can be gained by considering the motion of fluid through the secondary channel towards the main channel. As the fluid nears the intersection, it is accelerated by the main channel flow. We postulate that as the flows increase in velocity and the inertia of the main channel flow becomes more important, the dynamic pressure of the main channel flow is sufficient to distort the fluid in the secondary channel upwards away from the bottom of the channel. This in turn drives recirculation and causes mixing to occur. This parameter amounts to an effective Reynolds number for the inlet region that is distinct from the Reynolds number for fluid flow in the main channel defined in (2.2). The characteristic velocities U' in the secondary channel and U in the main channel can be expressed in terms of the main channel Reynolds number and the parameters listed in table 1:

$$U = \frac{n}{1+n}\frac{\mu Re}{\rho h}, \tag{3.1a}$$

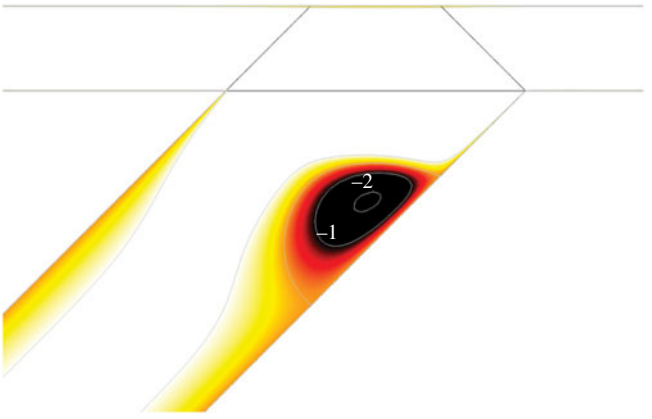

FIGURE 4. (Colour online) Dimensionless recirculation velocity, $\tilde{u}'$, in the x' direction in the inlet channel scaled by the characteristic secondary channel velocity U' for a main channel height of 100 μm, a secondary channel height of 250 μm, and a Reynolds number of 20. All other parameters are as described in table 1. Significant recirculation is observed, with a maximum negative dimensionless velocity in excess of −2.

$$U' = \frac{1}{1+n}\frac{\mu Re}{\rho h_{inlet}}. \tag{3.1b}$$

A simple scaling analysis of (2.1) operating in the x direction can be performed to derive the effective inlet Reynolds number, Re_{inlet}, in terms of the parameters listed in table 1, including the secondary channel angle α:

$$\begin{aligned} Re_{inlet} &= \frac{\rho\,(U - U'\cos\alpha)\,h}{\mu} \\ &= \left(\frac{n}{n+1} - \frac{h}{h_{inlet}}\frac{\cos\alpha}{n+1}\right) Re. \end{aligned} \tag{3.2}$$

It is also constructive to examine the magnitude of the recirculating velocity by considering the greatest negative velocity in the stagnation region in the $-x'$ direction scaled to the characteristic velocity scale in the secondary channel, U':

$$\tilde{u}' = \left|\min\left(\frac{u'}{U'}\right)\right|. \tag{3.3}$$

This quantity provides a measure of the extent to which recirculation is significant within the channel, and is illustrated in figure 4 for a demonstration case.

The inlet Reynolds number Re_{inlet} and the maximum dimensionless recirculation velocity $\tilde{u}'$ can then be tabulated over a wide range of conditions by varying the main channel Reynolds number and the secondary channel height. Figure 5 plots recirculation velocity as a function of inlet Reynolds number for a range of inlet heights and Reynolds numbers. This plot demonstrates that the value of Re_{inlet} at which recirculation becomes important, such that $\tilde{u}' > 1$, is a strong function of the relative heights of the channels, defined as $s = h_{inlet}/h$.

This result can be collapsed further by considering the relationship between the recirculation velocity $\tilde{u}'$, the relative heights of the secondary and main channels, s,

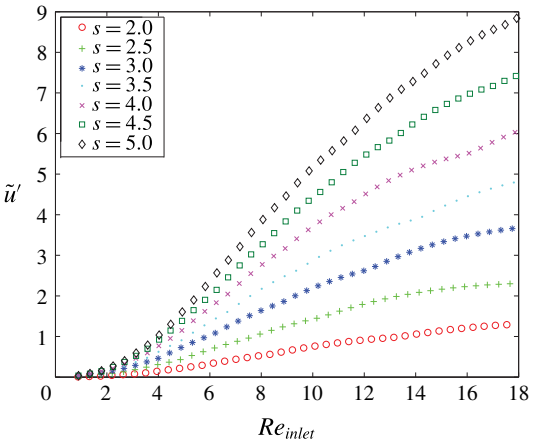

FIGURE 5. (Colour online) Maximum dimensionless recirculation velocity $\tilde{u}'$ as a function of inlet Reynolds number, Re_{inlet}, as defined in (3.2) for a range in relative height of the inlet channel s. Unless specified otherwise in the legend, all parameters are as listed in table 1.

the flow ratio n, and the inlet channel angle α. As either s or n gets larger, the velocity in the primary channel becomes larger relative to that of the secondary channel. From (3.1), the relationship between the flow ratio, the channel velocity scales, and the channel heights can easily be expressed:

$$\frac{U}{U'} = ns. \tag{3.4}$$

The fluid velocity in the main channel is the dominant source of fluid motion, and thus drives the recirculation. Since the recirculation effect is a result of the inertia in the primary channel, we expect that the dimensionless recirculation velocity $\tilde{u}'$ will increase as the primary channel velocity U increases. From (3.4), $U \sim ns$, so we expect a faster than linear increase in dimensionless recirculation velocity as the channel ratio h or flow ratio n is increased. It is therefore reasonable to consider the maximum recirculation velocity scaled to $(ns)^2$ as a good measure of recirculation. This expectation is validated by figure 6, which illustrates that the recirculation behaviour from 585 numerical simulations conducted by varying channel ratio, flow ratio, inlet angle, and inlet Reynolds number all collapse onto a single curve.

Although flow separation and recirculation play a key role in mixing, they are not the only source of non-idealities in the channel. It is customary to neglect edge effects for wide rectangular channels far from the walls, but those walls can play a very significant role when the flow bends at low or moderate Reynolds number, as observed in the case of Dean flow in a pipe or a rectangular channel (Dean 1927; Di Carlo 2009). Even at low Reynolds number, the walls can induce significant secondary flows around sharp corners or bends with a non-constant radius of curvature (Shankar 2000; Lauga, Stroock & Stone 2004; Guglielmini *et al.* 2010). The recirculating eddies formed in such geometries have been shown to induce the formation of biofilm streamers when certain strains of bacteria are introduced (Rusconi *et al.* 2010). Similar phenomena can be observed in contracting or expanding flows, which also have been shown to induce out-of-plane flow (Shankar 2000; Zhang *et al.* 2013).

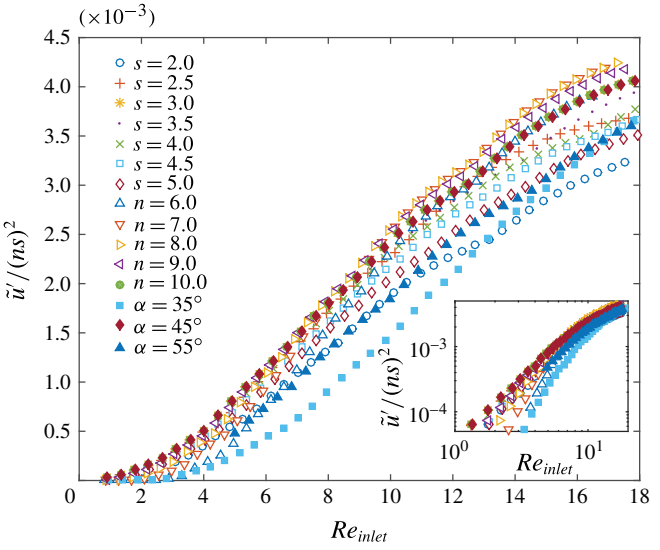

FIGURE 6. (Colour online) Maximum dimensionless recirculation velocity $\tilde{u}'$ scaled by $(ns)^2$, where n is the volumetric flow ratio, and s is the ratio of secondary to main channel height, as a function Reynolds number Re_{inlet} as defined in (3.2). All simulation parameters are as listed in table 1 except as listed in the legend. The inset plots the same data on a log–log scale.

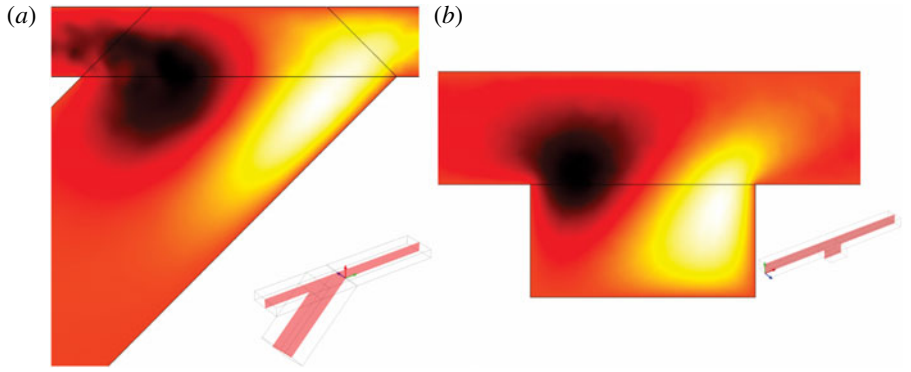

FIGURE 7. (Colour online) (*a*) Out-of-plane fluid flow velocity (surface) one quarter of the channel width away from the wall near the inlet of the three-dimensional channel with a height of 500 μm and a Reynolds number of 10. A schematic of the cut plane is shown as an inset. As the fluid in the main channel bends downwards towards the secondary channel, the fluid is deflected towards the centre of the channel, represented by the blue region. Likewise, the upwards curvature of the fluid as it bends back into the main channel results in fluid being driven towards the wall represented by the red region. (*b*) A similar effect can be observed for a simple rectangular channel with a square pocket added. The average fluid velocity and curvature are similar, so the out-of-plane behaviour is also very similar.

In the case of the inlet geometry considered here, velocity gradients between the centreline of the channel and the wall drives flow out of plane, further enhancing mixing as shown in figure 7. Interestingly, the effective curvature of the fluid flow

is not determined directly by the angle of the inlet, or the height of the channels, but by the deformation of the fluid flow as it curves upwards into the main channel. Figure 7(*b*) illustrates that the upwards curvature of the fluid, even in the absence of a secondary channel, contributes most strongly to the out-of-plane flow velocities. The net effect of the additional secondary flows is to enhance mixing further, with significant mass reaching the far wall of the channel even for channels as tall as 500 μm, as shown in figure 2. This channel height corresponds to an effective inlet Reynolds number of $Re_{inlet} = 14$. As the channel height is decreased further, the effective inlet Reynolds number will increase, increasing the recirculation effects. This result suggests that this value represents an upper bound on the effective inlet Reynolds number in order to suppress recirculation.

4. Conclusion

This work captures the dominant design criteria describing the convergence of two colaminar liquid streams at moderate Reynolds number in rectangular channels. We find that for any operating condition, the recirculation velocity can be written as a function of the channel aspect ratio, the flow ratio, and the inlet Reynolds number, $\tilde{u}'/(ns)^2 = F(Re_{inlet})$. This insight can be used as a guide for future channel designs, and informs the intuition that the velocity gradient of the fluid as it passes from the secondary channel into the main channel drives recirculation. A complete understanding of the source of the recirculation behaviour is beyond the scope of this work, and remains a promising avenue of future research.

In addition to the recirculation effect, we have also identified and numerically observed wall-induced eddy currents that produce out-of-plane fluid flow that enhance mixing and disrupt the assumption of two-dimensional flow, even for relatively wide channels. These two effects conspire to establish a maximum effective inlet Reynolds number to maintain the validity of the fully developed unidirectional flow assumption. The inlet Reynolds number must be considered to ensure the species separation necessary for a wide range of applications, including systems incorporating chemical and electrochemical reactions.

REFERENCES

BERGER, S. A., TALBOT, L. & YAO, L. S. 1983 Flow in curved pipes. *Annu. Rev. Fluid Mech.* **15**, 461–512.

BRAFF, W. A., BAZANT, M. Z. & BUIE, C. R. 2013*a* Membrane-less hydrogen bromine flow battery. *Nat. Commun.* **4**, 2346.

BRAFF, W. A., BUIE, C. R. & BAZANT, M. Z. 2013*b* Boundary layer analysis of membraneless electrochemical cells. *J. Electrochem. Soc.* **160** (11), A2056–A2063.

BRAFF, W. A., BUIE, C. R. & BAZANT, M. Z. 2013*c* Numerical and analytic modeling of a membraneless hydrogen bromine laminar flow battery. *ECS Trans.* **53** (7), 51–62.

CHIU, D. T. 2006 Cellular manipulations in microvortices. *Anal. Bioanal. Chem.* **387** (1), 17–20.

DEAN, W. R. 1927 Note on the motion of fluid in a curved pipe. *Phil. Mag.* **4** (20), 208–223.

DI CARLO, D. 2009 Inertial microfluidics. *Lab on a Chip* **9** (21), 3038–3046.

EYAL, S. & QUAKE, S. R. 2002 Velocity-independent microfluidic flow cytometry. *Electrophoresis* **23**, 2653–2657.

GAMBIN, Y., VANDELINDER, V., FERREON, A. C. M., LEMKE, E. A., GROISMAN, A. & DENIZ, A. A. 2011 Visualizing a one-way protein encounter complex by ultrafast single-molecule mixing. *Nat. Meth.* **8** (3), 239–241.

GUGLIELMINI, L., RUSCONI, R, LECUYER, S & STONE, H. A. 2010 Three-dimensional features in low-Reynolds-number confined corner flows. *J. Fluid Mech.* **668**, 33–57.

ISMAGILOV, R. F., STROOCK, A. D., KENIS, P. J. A., WHITESIDES, G. & STONE, H. A. 2000 Experimental and theoretical scaling laws for transverse diffusive broadening in two-phase laminar flows in microchannels. *Appl. Phys. Lett.* **76** (17), 2376–2378.

JAYASHREE, R. S., GANCS, L., CHOBAN, E. R., PRIMAK, A., NATARAJAN, D., MARKOSKI, L. J. & KENIS, P. J. A. 2005 Air-breathing laminar flow-based microfluidic fuel cell. *J. Am. Chem. Soc.* **127** (48), 16758–16759.

JAYASHREE, R. S., YOON, S. K., BRUSHETT, F. R., LOPEZ-MONTESINOS, P. O., NATARAJAN, D., MARKOSKI, L. J. & KENIS, P. J. A. 2010 On the performance of membraneless laminar flow-based fuel cells. *J. Power Sources* **195** (11), 3569–3578.

KENIS, P. J. A., ISMAGILOV, R. F. & WHITESIDES, G. M. 1999 Microfabrication inside capillaries using multiphase laminar flow patterning. *Science* **285** (5424), 83–85.

KUNDU, P. K., COHEN, I. M. & DOWLING, D. R. 2012 *Fluid Mechanics*, 5th edn. Academic.

LAUGA, E., STROOCK, A. D. & STONE, H. A. 2004 Three-dimensional flows in slowly varying planar geometries. *Phys. Fluids* **16** (8), 3051–3062.

MAO, X., NAWAZ, A. A., LIN, S.-C. S., LAPSLEY, M. I., ZHAO, Y., MCCOY, J. P., EL-DEIRY, W. S. & HUANG, T. J. 2012 An integrated, multiparametric flow cytometry chip using 'microfluidic drifting' based three-dimensional hydrodynamic focusing. *Biomicrofluidics* **6** (2), 24113–241139.

NASIR, M., MOTT, D. R., KENNEDY, M. J., GOLDEN, J. P. & LIGLER, F. S. 2011 Parameters affecting the shape of a hydrodynamically focused stream. *Microfluid. Nanofluid.* **11** (2), 119–128.

NOROUZI, M. & BIGLARI, N. 2013 An analytical solution for Dean flow in curved ducts with rectangular cross section. *Phys. Fluids* **25** (5), 053602.

RUSCONI, R., LECUYER, S., GUGLIELMINI, L. & STONE, H. A. 2010 Laminar flow around corners triggers the formation of biofilm streamers. *J. R. Soc. Interface* **7** (50), 1293–1299.

SALLOUM, K. S. & POSNER, J. D. 2010 Counter flow membraneless microfluidic fuel cell. *J. Power Sources* **195** (19), 6941–6944.

SHANKAR, P. N. 2000 On Stokes flow in a semi-infinite wedge. *J. Fluid Mech.* **422**, 69–90.

SPRAGUE, I. B. & DUTTA, P. 2012 Depth averaged analytic solution for a laminar flow fuel cell with electric double layer effects. *SIAM J. Appl. Maths* **72** (4), 1149–1168.

SUDARSAN, A. P. & UGAZ, V. M. 2006 Multivortex micromixing. *Proc. Natl Acad. Sci. USA* **103** (19), 7228–7233.

THORSON, M. R., BRUSHETT, F. R., TIMBERG, C. J. & KENIS, P. J. A. 2012 Design rules for electrode arrangement in an air-breathing alkaline direct methanol laminar flow fuel cell. *J. Power Sources* **218** (C), 28–33.

VAN HIRTUM, A., GRANDCHAMP, X. & CISONNI, J. 2012 Reynolds number dependence of near field vortex motion downstream from an asymmetrical nozzle. *Mech. Res. Commun.* **44**, 47–50.

ZHANG, J., LI, M., LI, W. H. & ALICI, G. 2013 Inertial focusing in a straight channel with asymmetrical expansion–contraction cavity arrays using two secondary flows. *J. Micromech. Microengng* **23** (8), 085023.